Effects of spatial resolution on WRF v3.8.1 simulated meteorology over the central Himalaya

Jaydeep Singh[1], Narendra Singh[1*], Narendra Ojha[2], Amit Sharma[3, a], Andrea Pozzer[4, 5], Nadimpally Kiran Kumar[6], Kunjukrishnapillai Rajeev[6], Sachin S. Gunthe[3], V. Rao Kotamarthi[7]

[1]Aryabhatta Research Institute of Observational Sciences, Nainital, India

[2]Physical Research Laboratory, Ahmedabad, India

[3]EWRE Division, Department of Civil Engineering, Indian Institute of Technology Madras, Chennai, India

[4]Department of Atmospheric Chemistry, Max Planck Institute for Chemistry, Mainz, Germany

[5]Earth System Physics Section, International Centre for Theoretical Physics, Trieste, Italy

[6]Space Physics Laboratory, Vikram Sarabhai Space Centre, Thiruvananthapuram, India

[7]Environmental Science Division, Argonne National Laboratory, Argonne, Illinois, USA

[a]Now at Department of Civil and Infrastructural Engineering, Indian Institute of Technology Jodhpur, Jodhpur, India

Correspondence: Narendra Singh (narendra@aries.res.in) and Andrea Pozzer (andrea.pozzer@mpic.de)

Abstract

The sensitive and fragile ecosystem of the central Himalayan (CH) region, experiencing enhanced anthropogenic pressure, requires adequate atmospheric observations and an improved representation of Himalaya in the models. However, the accuracies of atmospheric models remain limited here due to highly complex mountainous topography. This article delineates the effects of spatial resolution on the modeled meteorology and dynamics over the CH by combining the WRF (Weather Research and Forecasting) model with the GVAX (Ganges Valley Aerosol Experiment) observations during the summer monsoon. WRF simulation is performed over a domain (d01) encompassing northern India at 15 km x 15 km

resolution, and two nests: d02 (5 km x 5 km) and d03 (1 km x 1 km) centered over CH with boundary conditions from respective parent domains. WRF simulations reveal higher variability in meteorology e.g. Relative Humidity (RH=70.3–96.1%), Wind speed (WS=1.1–4.2 ms^{-1}), as compared to the ERA Interim reanalysis (RH=80.0–85.0, and WS=1.2–2.3ms^{-1}) over the northern India owing to higher resolution. WRF simulated temporal evolution of meteorological profiles is seen to be in agreement with the balloon-borne measurements with stronger correlations aloft (r = 0.44–0.92), than those in the lower troposphere (r = 0.18–0.48). However, the model overestimates temperature (warm bias by 2.8^{o}C) and underestimates RH (dry bias by 6.4%) at surface in the d01. Model results show a significant improvement in d03 (P=827.6 hPa, T=19.8^{o}C, RH=92.3%) and are closer to the GVAX observations (P=801.4, T=19.5, RH=94.7%). Interpolating coarser simulation (d01, d02) to the altitude of station reduces the biases in pressure and temperature, however, suppresses the diurnal variations highlighting significance of well-resolved terrain effects (d03). Temporal variations in near-surface P, T and RH are also reproduced by WRF d03 to an extent (r > 0.5). A sensitivity simulation incorporating the feedback from nested domain demonstrated improvements in simulated P, T and RH over CH. Our study shows the WRF model set up at finer spatial resolution can significantly reduce the biases in simulated meteorology and such an improved representation of CH can be adopted through domain feedback into regional-scale simulations. Interestingly, WRF simulates a dominant easterly wind component at 1 km x 1 km resolution (d03), which was missing in the coarse simulations; however, a frequent southeastward wind component remained underestimated. Model simulation implementing a high resolution (3 s) topography input (SRTM) improved the prediction of wind directions, nevertheless, further improvements are required to better reproduce the observed local-scale dynamics over the CH.

1. Introduction

Himalayan region is one of the most complex and fragile geographical systems in the world, and has paramount importance for the climatic implications and air composition at regional to global scales (e.g.

Lawrence et al., 2010, Pant et al., 2018; Lelieveld et al., 2018). The ground-based observations of meteorology and fine-scale dynamics are highly sparse. In this direction, an intensive field campaign called as the GVAX (Kotamarthi, 2013) was carried out over a mountainous site in the Central Himalaya which provided valuable meteorological observations for atmospheric research, model evaluation and improvements. Accurate simulations of meteorology are needed for numerous investigations, such as to study the regional and global climate change, snow-cover change, trapping and transport of regional pollution, and the hydrological cycle especially monsoon system (e. g. Sharma and Ganju, 2000; Bhutiyani et al., 2007; Pant et al., 2018). Studies focussing over this region have become more important due to the increasing anthropogenic influences resulting in enhanced levels of Short-Lived Climate forcing Pollutants (SLCPs) along the Himalayan foothills (e. g. Ojha et al., 2012; Sarangi et al., 2014; Rupakheti et al., 2017; Deep et al., 2019; Ojha et al., 2019). Although Global Climate Models (GCMs) simulate the climate variabilities over global scale, their application for reproducing observations in the regions of complex landscapes is limited, due to coarse horizontal resolution (e. g. Wilby et al., 1999; Boyle et al. 2010; Tselioudis et al., 2012; Pervez and Henebry, 2014; Meher et al., 2017). Mountain ridges, rapidly changing land-cover, and the low altitude valleys often lie within a grid box of typical global climate models resulting in significant biases in model results when compared with observations (e. g. Ojha et al., 2012; Tiwari et al., 2017, Pant et al., 2018). On the other hand, Regional Climate Models (RCMs) at finer resolutions allow better representation of the topographical features thus providing improved simulations of the atmospheric variability over regions of complex terrains. Several mesoscale models (e. g. Christensen et al., 1996; Caya and Laprise 1999; Skamarock et al., 2008; Zadra et al., 2008) have been developed and applied successfully over different parts of the world. These studies have revealed that the RCMs provide significant new insights by parameterizing or explicitly simulating atmospheric processes over finer spatial scales. Nevertheless, large uncertainties are still seen over highly complex areas indicating the effects of further unresolved terrain features (e. g. Wang et al., 2004; Laprise, 2008; Foley, 2010) and need to improve the simulations.

Of late, anthropogenic influences and climate forcing have been increasing over the Himalaya and its foothill regions since pre-industrial times (Pant et al., 2006; Bonasoni et al., 2012; Srivastava et al., 2012). Further, an increase in the intensity and frequency of extreme weather events have been observed over the Himalayan region (e. g. Nandargi and Dhar, 2012; Sun et al., 2017; Dimri et al., 2017) in past few decades. These events include extreme rainfall and resulting flash floods, cloudbursts, landslides etc., and their causes range from mesoscale processes to larger synoptic scale events. Unfortunately, the lack of observational network covering the Himalaya and foothills with sufficient spatio-temporal density inhibits the detailed understanding of the aforementioned processes, and meteorological and dynamical conditions in the region. Therefore, usage of regional models, evaluated against available in-situ measurements would fill the gap of investigating atmospheric variability in the observationally sparse and geographically complex mountain terrain of Himalaya.

The biases in simulating the meteorological parameters especially in the lower troposphere are associated with several factors e.g. representation of topography, land use, surface heat and moisture flux transport, and parameterization of physical processes (e. g. Lee et al., 1989; Hann and Yang, 2001; Cheng and Steenburgh, 2005; Singh et al., 2016). WRF model has been applied over the complex terrains in the Himalaya region (e.g. Sarangi et al., 2014; Singh et al., 2016, Mues et al., 2018; Wang et al., 2020), Tibetan Plateau (e.g. Gao et al., 2015; Zhou et al., 2018), and intermountain west of the United States (e.g. Zhang et al., 2013) to evaluate and study the meteorology and dynamics. A cold bias was reported in this model over the Tibetan Plateau and Himalayan region by Gao et al (2015). Near surface winds showed biases linked with unresolved processes in the model such as sub-grid turbulence, land-surface atmospheric interactions, besides boundary layer parametrization (Hanna and Yang, 2001; Zhang and Zheng, 2004; Cheng and Steenburgh, 2005). Zhou et al., (2018) found lower biases in simulated winds after taking into account the turbulent orographic form drag over the Tibetan Plateau.

WRF model with suitably chosen schemes has been shown to reproduce the regional-scale meteorology (Kumar et al., 2012) and to some extent also the mountain-valley wind systems (Sarangi et al., 2014) and

boundary layer dynamics (Singh et al., 2016; Mues et al., 2018) over the Himalayan region. Nevertheless local meteorology is still difficult to simulate correctly; Mues et al (2018) performed high resolution WRF simulation over Kathmandu valley of Himalaya and reported overestimation of 2m temperature and 10m wind speed attributed to complex topography even at resolution of 3 km x 3 km. Meteorological simulations including winds and precipitation were shown to improve with increase in grid resolution over different parts of the world (e.g. Mass et al., 2002; Rife and Davis, 2005; Hart et al., 2005).

Most of the studies carried out over the Himalayan region applied model at coarse horizontal resolutions (45 to 30 km) and evaluated simulations over larger spatial scales, except the study by Mues et al. (2018) which used relatively higher spatial resolution (3 km x 3 km). Nevertheless, it remains unclear how the finer resolution could better resolve the complex terrain of the central Himalaya and improve the meteorological simulations, especially at 5 km to 1 km resolution.

With this opportunity of model evaluation and improvements in simulating meteorological and dynamical variability over the CH, here, we have used a nested WRF set up with a coarse 15 km x 15 km domain (d01) with nests of 5 km x 5 km (d02) and 1 km x 1 km (d03) centred over the CH. The main objectives of the study are as follows:

1. To examine the model performance over the CH at 15 km x 15 km resolution
2. To examine the effects or improvements that can be achieved at higher spatial resolutions: 5 km x 5 km, and 1 km x 1 km.
3. To investigate the effect of feedback from nest that could be adopted into parent domain, as this would allow configuring a setup covering larger Indian region with more accurate results over Himalaya
4. To implement a very high resolution (3 s) topographical input into the model to examine the potential of simulations finer than 1 km in reproducing local-scale dynamics

Subsequent section 2 describes the model set up, followed by experimental design, and a discussion of datasets used for model evaluation. Section 3 provides comparison of model results with the ERA Interim reanalysis (section 3.1), radiosonde observations (section 3.2), and ground-based measurements (section 3.3). Analysis of domain feedback is presented in section 3.4, and the effect of implementing high-resolution topography is investigated in section 3.5, followed by the summary and conclusions in section 4.

2. Methodology

2.1 Model set up and Experimental Design

Weather Research and Forecasting (WRF) model–version 3.8.1 has been used in the present study. WRF is a mesoscale non-hydrostatic, Numerical Weather prediction (NWP) model with advance physics and numerical schemes for simulating meteorology and dynamics. WRF-ARW uses Eulerian mass based dynamical core with terrain-following vertical coordinates (Skamarock et al., 2008). ERA Interim reanalysis from the European Center for Medium Range Weather Forecasts (ECMWF) available at a horizontal resolution of 0.75^0 x 0.75^0 at 6 h interval has been used to provide the initial and lateral boundary conditions to the WRF model (Dee et al., 2011). Static geographical data, which includes the information of terrain height, land use, and land cover etc., is based on the Moderate Resolution Imaging Spectroradiometer (MODIS) data available at 30s horizontal resolution.

The shortwave radiation scheme used is the Goddard scheme (Chou and Suarez, 1994) while the long wave radiation is simulated by the Rapid Radiative Transfer Model (Mlawer et al., 1997) scheme. For resolving the boundary layer processes the first order nonlocal closure based Yonsei University (YSU) scheme (Hong et al., 2006) is used including an explicit entrainment layer with the K-profile in an unstable mixed layer. PBL height is determined from the Richardson number (Ri_b) method in this PBL scheme. Convection is parameterized by the Kain-Fritsch (KF) cumulus parameterization (CP) scheme, accounting for sub-grid level processes in the model such as precipitation, latent heat release and vertical redistribution

146 of heat and moisture as a result of convection (Kain, 2004). With increase in model grid resolution to less
147 than 10 km (known as "grey area"), the CP scheme is usually turned off and an explicit microphysics (MP)
148 scheme is needed to resolve cloud and precipitation processes (Weisman et al., 1997). In the present study,
149 the CP scheme is used for d01 while it is turned off for d02 and d03. The Thomson microphysics containing
150 prognostic equations for cloud water, rain water, ice, snow, and graupel mixing ratios, is used (Thompson
151 et al., 2004). Parameterization of surface processes is done with MM5 Monin-Obukhov scheme and
152 Unified Noah land surface model (LSM) (Chen and Dudhia, 2001; Ek et al., 2003; Tewari et al., 2004).
153 The Noah LSM includes a single canopy layer and four soil layers at 0.1, 0.2, 0.6 and 1m within 2m of
154 depth (Ek et al., 2003).

155 The model is configured with three domains of 15 km (d01), 5 km (d02) and 1 km (d03) horizontal grid
156 spacing using Mercator projection centering at Manora Peak (79.46^{o}N, 29.36^{o}E, amsl ~ 1936m) in central
157 Himalaya. Topography within the model domains is highly complex as evident form the ridges (Figure 1).
158 Outer domain d01 includes north part of Thar Desert, part of IGP (Indo-Gangetic-Plain), Himalayan
159 mountains with vegetation and snow cover, while the innermost domain d03 consists of mostly
160 mountainous terrain. Model atmosphere has 51 vertical levels with top at 10 hPa. For d01, 100 east-west
161 and 86 north south grid points are used to account for the effect of synoptic scale meteorology e.g. Indian
162 summer monsoon. The d02 has 88 east-west and 76 north-south grid points covering sufficient spatial
163 region around the observational site to consider the effects of mesoscale dynamics, e.g. change of wind
164 pattern due to orography. The innermost domain 03 has 126 east-west and 106 north-south grid points
165 mainly to reveal local effects e.g. convection, advection, turbulence, orthographic lifting etc.

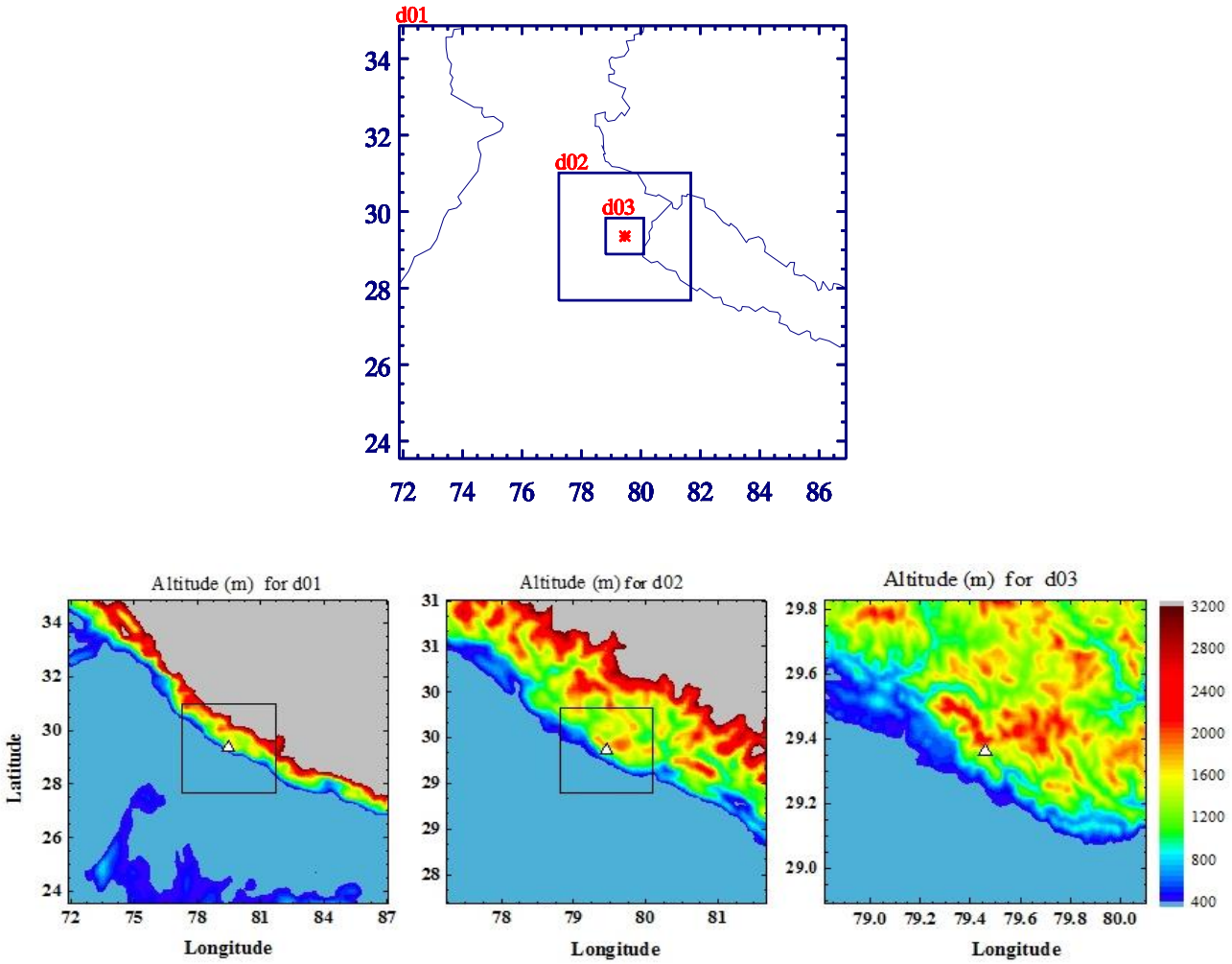

166

167

168 **Figure 1:** Topography in WRF model domains at three horizontal resolutions: domain d01 (15 x 15km),
169 domain d02 (5 x 5km) and domain d03 (1 x 1 km). Triangle symbol indicates the location of the GVAX
170 campaign over Manora Peak, Nainital. Box inside the figure represents the nested domain.

171 The d01 simulation provides the boundary conditions to domain d02, and domain d02 to innermost domain
172 d03. For d01, boundary conditions are provided from ERA Interim reanalysis, as explained earlier. Model
173 simulation has been performed for four months of the summer monsoon season: 01 June 2011 to 30
174 September 2011 (JJAS). First 10 days of the simulation is considered as the spin-up and removed from the
175 analysis. Only the outer domain d01 is nudged with the global reanalysis for temperature, water vapor,
176 zonal and meridional (u and v) components of wind with nudging coefficient of 0.0006 (6 x 10^{-4}) at all
177 vertical levels (e.g. Kumar et al., 2012). Several of the configuration options e. g. physics, meteorological

nudging, etc. are selected following earlier applications of this model over this region (e. g. Kumar et al., 2012; Ojha et al., 2016; Singh et al., 2016; Sharma et al., 2017).

2.2. Observational data

We utilize the observations conducted as a part of an intensive field campaign- the Ganges Valleys Aerosol Experiment (GVAX) for the evaluation of model simulations. The GVAX campaign was conducted using Atmospheric Radiation Measurement (ARM) Climate Research Facility of the U.S. Department of Energy (DOE) from June, 10 2011 to March 31, 2012 at ARIES, Manora Peak in Nainital (e.g. Kotamarthi, 2013; Singh et al., 2016; Naja et al., 2016). The surface-based meteorological measurements of ambient air temperature, pressure, relative humidity, precipitation, wind (speed and direction) were carried out using an automatic weather station at 1-minute temporal resolution. The instantaneous values of the observations are compared with hourly instantaneous model output at the nearest grid point.

The vertical profiles of temperature, pressure, relative humidity and horizontal wind (speed and direction) were measured by four launches (00:00, 06:00, 12:00 and 18:00 UTC) of the radiosonde each day during the campaign (Naja et al., 2016). The continuous vertical profiles of the meteorological parameters except wind speed and direction were available from end of June 2011 to the entire period of study, whereas valid wind data were available only for September 2011. Hence, in this study, radiosonde measurements from July 1, 2011 onwards are used for model evaluation of meteorological parameters, except wind speed and direction, which are evaluated for the month of September. A total of 309 valid profiles of temperature and relative humidity and 104 profiles of wind are used. The statistical metrics mean bias (MB), root mean square error (RMSE) and correlation coefficient (r) are used for the model evaluation and the description of these metrics is given in the supplementary material.

3. Results and Discussions

3.1. Comparison with ERA Interim reanalysis

ERA Interim reanalysis data set is available globally at resolution of 0.75^0 x 0.75^0 with 37 vertical levels from surface to the top at 1 hPa with covering time period from 1979 to present at 6-hourly time step (Dee et. al., 2011). Here, we have used the ERA Interim data available at 0.75^o x 0.75^o for comparison with WRF results. We first compare the WRF simulated spatial distribution of meteorological parameters (surface pressure, 2m air Temperature, 2m RH and 10m WS) with ERA Interim reanalysis over common area of all the domains and averaged for the complete simulation period (Figure 2). The common area in all domains includes low-altitude Indo-Gangetic Plain (IGP) region in south (with elevation of less than 400m, Figure 1) and elevated mountains of the central Himalaya in north. Also, for a consistent comparison, model simulated values are taken at the same time intervals as that in ERA Interim data (i.e. every 6h). From the comparison Figure 2, it is evident that the meteorological parameters simulated by the model are dependent on the model grid resolution. The existence of the sharp gradient topographic height (SGTH) of about 1600 m from the foothill of the Himalaya to the observational site modifies the wind pattern as well as moisture content differently at different grid resolutions, indicating the critical role of mountain orography. The surface pressure explicitly depends upon the elevation of a location from mean sea level. The contour plot of the pressure from ERA Interim shows surface pressure of about 900hPa for observational site Manora Peak and varied from 550 to 975 hPa within this region, while WRF simulated pressure is 869 hPa, 835hPa and 827 hPa for d01, d02 and d03, respectively. WRF simulated surface pressure ranges from 821.9 hPa over high altitude CH region to 977.0 hPa in IGP region within d01. At the same time, the variation range of surface pressure is 788.1 – 977.5 and 760.4–977.7 hPa within d02 and d03 respectively, and the minimum pressure decreases from d01 to d03 which is attributed to the improvement in resolved topography on increasing model grid resolution. The effects of the SGTH are not clearly observed for temperature, wind and RH in ERA-Interim contours, and it could be due to the unresolved topographic features. Simulated spatial profiles show significantly distinct meteorology in

Indo-Gangetic Plain (IGP), which lies just in the foothills of Himalaya, and elevated central Himalayan region.

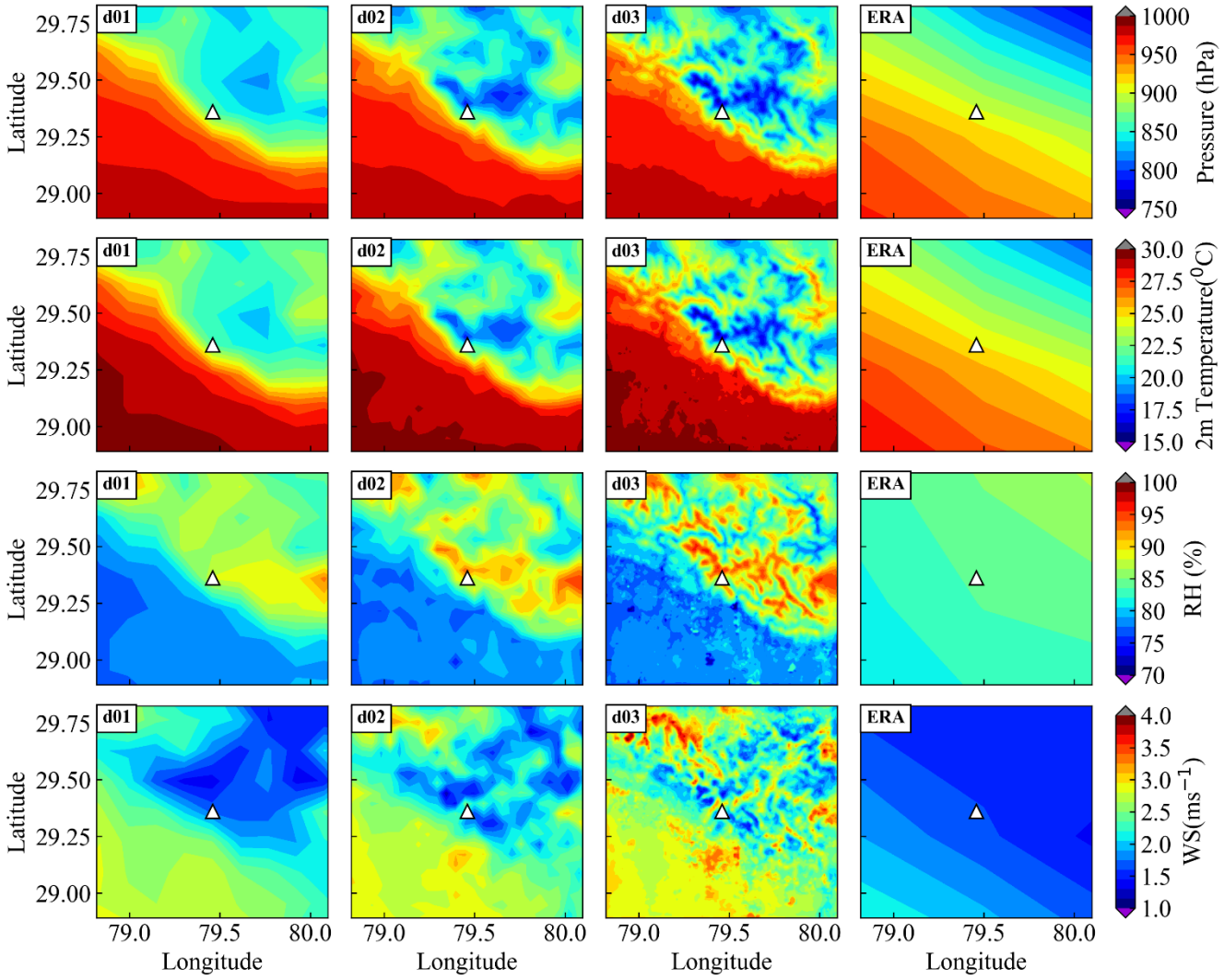

Figure 2. Contours in the first three columns show WRF results for the three domains (first column: d01, second column: d02 and third column: d03) and the fourth column shows corresponding parameters from the ERA Interim reanalysis. First row shows mean surface pressure during the monsoon (JJAS), second row shows 2m temperature (in ^{0}C), 3rd row shows 2m relative humidity (RH; %) and bottom row shows 10 m wind speed (WS; ms^{-1}).

The effect of spatial resolution is clearly observed over the mountainous region of Himalaya, where size of the mountains changes abruptly, with the modelled output showing distinct features with increasing

grid resolution. On the other hand, there are minimal differences in the topography of the IGP, and hence features are well captured in the model even at coarser resolution of 15 Km.

Model simulations show topography dependent spatial variation in the 2m temperature in the ranges of 20.0–29.5^{0}C in d01,17.3–29.6^{0}C in d02, and 15.5.0–29.9^{0}C in d03 with lowest values simulated over the elevated mountain peaks and higher values over the temperate IGP region. The contours in three model domains show explicit dependency of 2m temperature on the grid resolution over the mountainous region. With increasing model resolution, the topography is resolved to a greater extent and the lower temperature is simulated at higher surface elevations, as expected. Estimation of water vapour is very important for both climate and numerical weather prediction (NWP) applications. The relative humidity is above 70% in all three domains as the study period is monsoon season. The variations (minimum-maximum) in the relative humidity in ERA-Interim (80% to 85%) data sets, domains d01 (77-93%), d02 (74 – 95%), and d03 (70- 96%) are generally comparable. The mountain slopes provide the uplift to the monsoonal moist air that subsequently saturates on ascent and increases the relative humidity to about 90% as observed over the grid encompassing the site.

The wind speed is highly dependent upon the model grid resolution as well as orography-induced circulations during different seasons (Solanki et al., 2016; Solanki et al 2019) as shown in Figure 2. As mentioned earlier, although the topography of the IGP region does not vary abruptly, the magnitude of the wind speed over this region as well as over the complex Himalayan region are found to change significantly at different model resolutions, thereby indicating that the wind speed is very sensitive to both model resolution and topography. The wind speed in d01 varies from minimum value of 1.3 ms^{-1} to maximum value of 2.8 ms^{-1}, while the wind variations in domains d02 (1.2 – 3.4 ms^{-1}) and d03 (1.3 – 4.2 ms^{-1}) overestimated as compared to the ERA-interim (1.2–2.3ms^{-1}). Overall, the variations in surface pressure, temperature, and relative humidity are seen to be similar between the two datasets.

3.2. Comparison with Radiosonde observations

Model simulated vertical structure of temperature, relative humidity, and wind speed are evaluated against the radiosonde observations during the GVAX campaign. Such comparisons from surface to 50 hPa are shown in the Figure 3a-c for WRF d01 simulation and the radiosonde observations in the Figure 3d-f.

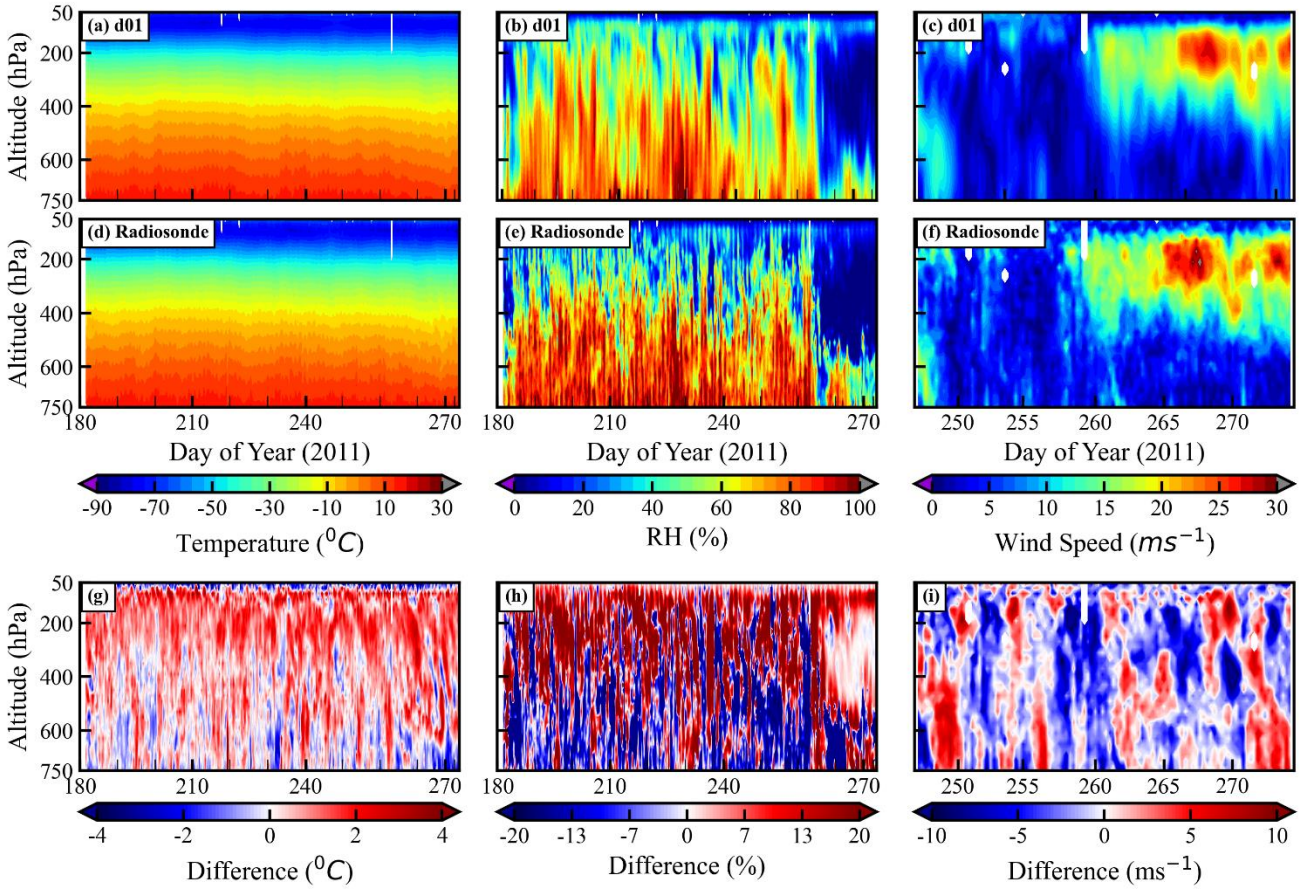

Figure 3: The comparison of **(a)** temperature in ^{0}C, **(b)** relative humidity (RH; %), and **(c)** wind speed in ms^{-1} (c) vertical profiles in WRF simulation d01 with the radiosonde observations (d, e, and f). The x-axis of (a), (b), (d), (e), (g) and (h) show the day of the year 2011 starting from 1 July (182nd day) to 30 September (273rd day). Wind speed profiles (c, f) in ms^{-1} are plotted only for month September, 2011. The third row (g, h, and i) shows the difference in temperature, relative humidity, and wind speed between WRF d01 simulation and radiosonde observation.

The inversion of the temperature at the top of the troposphere occurred at ~90hPa (~16km) in observations. Radiosonde profiles (Figure 3a) show that temperature decreases with pressure from 15.5^{0}C at 750 hPa to

-78.0 ^{0}C at ~90 hPa. Mean temperature profile simulated by the WRF model also captures this variability showing a reduction from 15.1 ^{0}C to -76.6 ^{0}C in these pressure levels. Further the difference between model (d01) and radiosonde observations (Figure 3g) are found in the range of -4 to 4^{0}C. The mean RH values from the radiosonde observation (model d01) also show decrease from 82.3% (76.7%) at 750 to 25.2% (32.0%) at 90 hPa. The difference of the mean RH between observation and model (Figure 3h) shows that model simulates wetter (or more humid) atmosphere at higher altitudes while showing a dry bias in lower altitudes. The observations of wind speed from radiosonde were available only from 01 September 2011 onwards therefore wind comparison is made only for the September month. The simulated profiles of the wind agree generally well with the observations. Wind speed is observed less than 10 ms^{-1} up to 400 hPa over the month of September and similar magnitude is observed above 400 hPa till mid of September (day of year 258). Further, the wind speed observed ≥15 ms^{-1} above 400hPa after 258 day of year (15 September). The vertical variation of wind speed well simulated by model. For the statistical comparison of the simulated meteorology with the observations, the Taylor diagram (Taylor, 2001) is used and shown in Figure 7a. In the diagram the comparison is summarized with correlation coefficient (r), normalized root mean squared difference (RMSD) and normalized standard deviation (SD), normalized to the standard deviation of observation. In most of the cases, model simulates less variability in meteorological parameters as shown by the normalized standard deviation which turns out to be less than 1. For temperature and wind speed, model shows good agreement at 250hPa ($r > 0.80$) than that in lower altitudes i.e. 750hPa ($r < 0.40$). On the other hand, model captures variability in humidity relatively well at 500 hPa ($r = 0.71$) but shows poor correlation at 50 hPa ($r = 0.17$) near the model top.

Lower correlations for temperature and wind speed near to the surface (750 hPa) could be due to the terrain induced effects most significant in the local boundary layer. The, surface level winds, and turbulence etc. are some of the features of the boundary layer that are largely affected by the surface and terrain characteristics. The vertical profiles of these parameters for all three model domains only up to 500 hPa is shown in Figure 4. Differences between the simulated vertical profile of temperature and radiosonde

observation below 500hPa (Figure 4) are in general similar in all the domains. Except for the relative humidity in d01, other meteorological parameters shown here do not reveal strong dependencies on the model resolution. Model however overestimates the relative humidity near 500hPa level in d02 and d03 on some of the days. In case of the wind speed, the model underestimates the magnitude of the wind in first few days up to 500 hPa, though qualitatively the model is able to capture the vertical profiles.

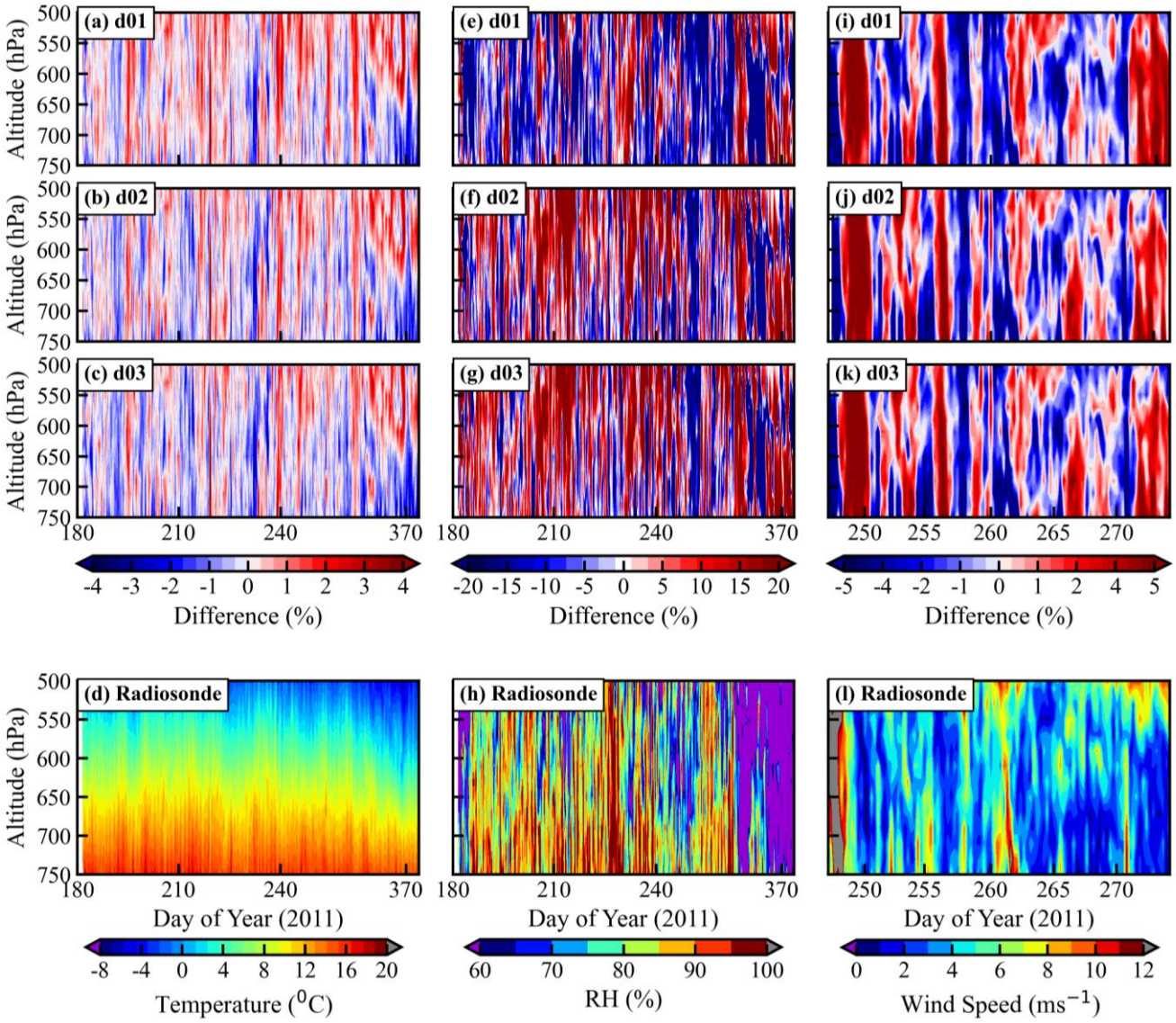

Figure 4: Difference between model (d01: first row, d02: second row, d03: third row) and radiosonde observation for temperature (first column: a, b, c), relative humidity (second column: e, f, g) and wind speed (third column: i, j, k) profiles up to 500 hPa. Radiosonde observations are also shown (fourth row).

The x-axis of (a-h) shows the day of the year 2011 from 1 July (182nd day) to 30 September (273rd day). Wind speed (ms^{-1}) profiles (i-l) are plotted only for the month September, 2011.

Figure 5 shows the vertical profiles of the statistical metrics: mean bias (MB), root mean square error (RMSE), and correlation coefficient (r) for temperature, relative humidity, and wind speed for the three simulations (d01, d02, d03). The magnitude of the MB values throughout the troposphere are estimated to be within about 1 ^{o}C, 12 %, 2.5 ms^{-1} for temperature, relative humidity, and wind speed, respectively. Additionally, RMSE values are about 1 ^{o}C, 15–30%, and 2.5–5 ms^{-1} for temperature, relative humidity, and wind speed, respectively. As discussed earlier also, correlations between model results and observations are found to be stronger in the middle and upper troposphere as compared to the lower troposphere. For temperature, the r values are higher than 0.75 between 600 to 200 hPa, whereas it decreases up to 0.4 at lower altitudes i.e. near 800 hPa. Correlations in lower troposphere are particularly weaker (r = ~0.25) in case of wind speed. The results suggest that model captures well the day-to-day variabilities in the meteorological parameters in the middle upper troposphere and to a minor extent in the lower troposphere. Relatively weaker correlations in the lower troposphere are suggested to be associated with more pronounced effects of the uncertainties caused by the underlying complex mountain terrain and resulting unresolved local effects. Wind fields near the surface have been shown to be strongly impacted by interactions between terrain and boundary layer besides orographic drag in a modelling study over the Tibetan Plateau (Zhou et al., 2018) and in measurements over Himalaya (Solanki et al., 2019). Increase in bias with altitude was reported by Kumar et al (2012) for dew point temperature. Besides the model physics, the higher uncertainties in radiosonde observations of humidity also contribute to these differences. The effect of model resolution is not very significant for temperature and wind profiles above 800 hPa, nevertheless, the mean bias in RH is lower in d02 and d03 simulations (~5%) in the 800–600 hPa. Overall, it is seen that model captured the vertical structures of meteorological parameters, however, better representation of complex terrains itself is insufficient for improving the model performance aloft. This highlights the need of future studies evaluating various physics schemes on top of better topography

representation considered here. Nevertheless, model biases have been significantly reduced for surface level meteorology with higher resolution, which is discussed in detail in the next section (3.3).

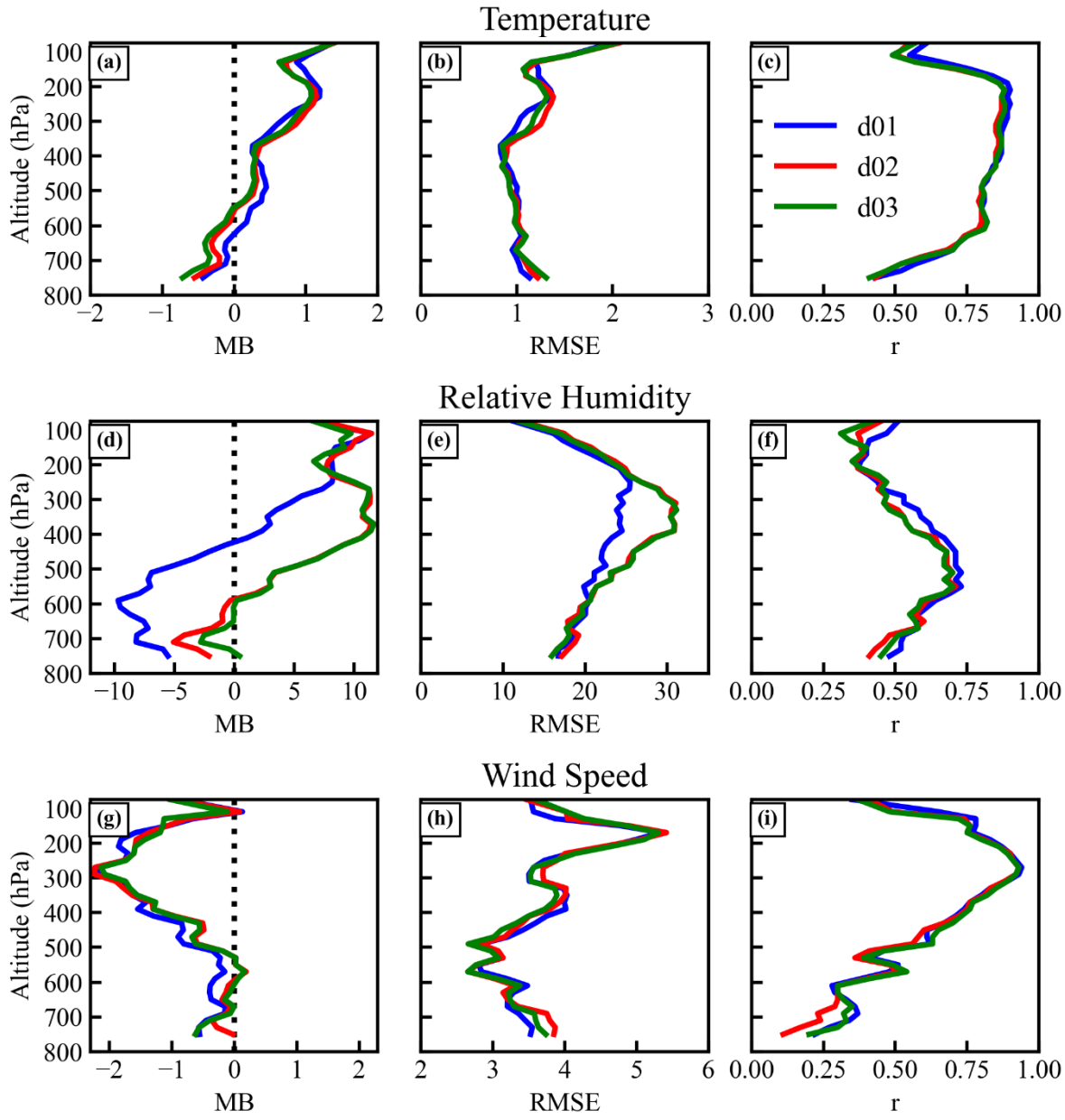

Figure 5. The vertical profiles of mean bias (MB), root mean square error (RMSE), and correlation coefficient (r) for temperature, relative humidity, and wind speed for different domains d01 (blue), d02 (red) and d03 (green).

3.3. Comparison with ground-based observations

Model simulated 2m temperature (T2), 2m relative humidity (RH2) and 10 m wind speed (WS10) for the observational site, Manora Peak are compared with the ground-based measurements made during GVAX campaign in Figure 6 and summarized in Table1. The diurnal variations in T2, RH2 and WS10 simulated by the WRF model are compared with observations, whereas the surface pressure does not show a significant diurnal variation (not shown here). Model simulation d01 shows a positive bias of 68 hPa in surface pressure with strong correlation (r = 0.97) with observation (mean = ~801 hPa). A significant improvement is achieved (MB = 26 hPa) in d03 i.e. the finest resolution simulation (Figure 6b and Table 1). WRF model simulated T2 shows warm bias in all the three domains. The simulated T2 for d01 varies from 16.2 to 28.7 ^{0}C with the higher mean value of 22.3±2.1^{0}C compared to observed mean value of about 19.5±1.6^{0}C with a correlation of r = 0.75 between d01 and observation. This warm bias is seen to decrease from d01 (2.8 ^{0}C) with increasing model resolution to 0.2^{0}C in the d03 simulation (Table S1). The mean value of the RH2 in d01 is about 88.2±9.7% lower by 6.4% lower than the observed value 94.7±9.5% with the correlation about 0.45 (Figure 7bs). MB and RMSE values of RH2 show a decrease with increasing model resolution (Table S1). As relative humidity also depends on temperature therefore the diurnal variation in 2m specific humidity (Q2; gkg^{-1}) has also been analyzed (Figure S1). Q2 is observed in the range of 5.5–21.5 g kg^{-1} with mean value as 16.8±2.0 g kg^{-1}. It is found that the agreement in Q2 is relatively better (MB = -0.7; r = 0.77 in d03), when the statistical metrics are compared with that for RH (Table S1). The wind speed plays a vital role in transport processes and controls the dynamics of the atmosphere at different temporal and spatial scales. The average 10m wind speed (WS10) over the measurement station is about 2.1±1.4 ms^{-1} which is similar in d01 (2.1±1.1) while overestimated in d02 by 0.9 ms^{-1} and 0.5 ms^{-1} d03 (Table 1 and Table S1). The correlation in case of the WS10 is 0.18 in d01 and d02 which improves to 0.24 in d03. The diurnal variation of WS10 (Figure 6c) is not well captured especially during the noontime.

Table 1: Mean values along with minimum and maximum of the meteorological parameters: surface pressure (P; hPa), 2m Temperature (T2; ^{0}C); 2m relative humidity (RH2; %) and 10m wind speed (WS10; ms^{-1}) in the model simulations and observations. An additional evaluation is presented accounting for the difference in model surface altitude and actual altitude of measurements (referred to as with altitude adjustment).

Parameter	**Without altitude adjustment**			**With altitude adjustment**			**Observation**
	d01	**d02**	**d03**	**d01**	**d02**	**d03**	
P (hPa)	869.6±2.6	835.3±2.5	827.6±2.4	801.3±2.4.6	801.3±2.4	801.4±2.4	801.1±2.4
Min/Max	862.8/875.1	828.3/840.8	821.2/833.1	795.0/806.7	795.0/806.7	795.2/806.8	795.1/806.8
T2 (^{0}C)	22.3±1.8	20.4±1.8	19.8±1.1	18.4±0.8	18.4±0.9	18.3±0.9	19.5±1.1
Min/Max	16.2/28.7	15.1/26.0	14.0/25.0	16.1/20.9	15.5/21.8	15.6/22.1	14.8/25.6
RH2(%)	88.2±9.7	94.3±6.4	92.3±7.9	86.2±10.9	93.8±8.5	91.5±9.7	94.7±9.5
Min/Max	53.3/100	67.6/100	52.3/100	43.9/100	51.3/100	47.9/100	31.6/100
WS10 (ms^{-1})	2.1±1.1	3.0±1.4	2.6±1.7	3.4±2.6	4.8±3.1	4.0±3.1	2.1±1.4
Min/Max	0.0/8.6	0.1/11.4	0.1/11.7	0.0/20.2	0.1/23.9	0.1/22.1	0.0/10.0

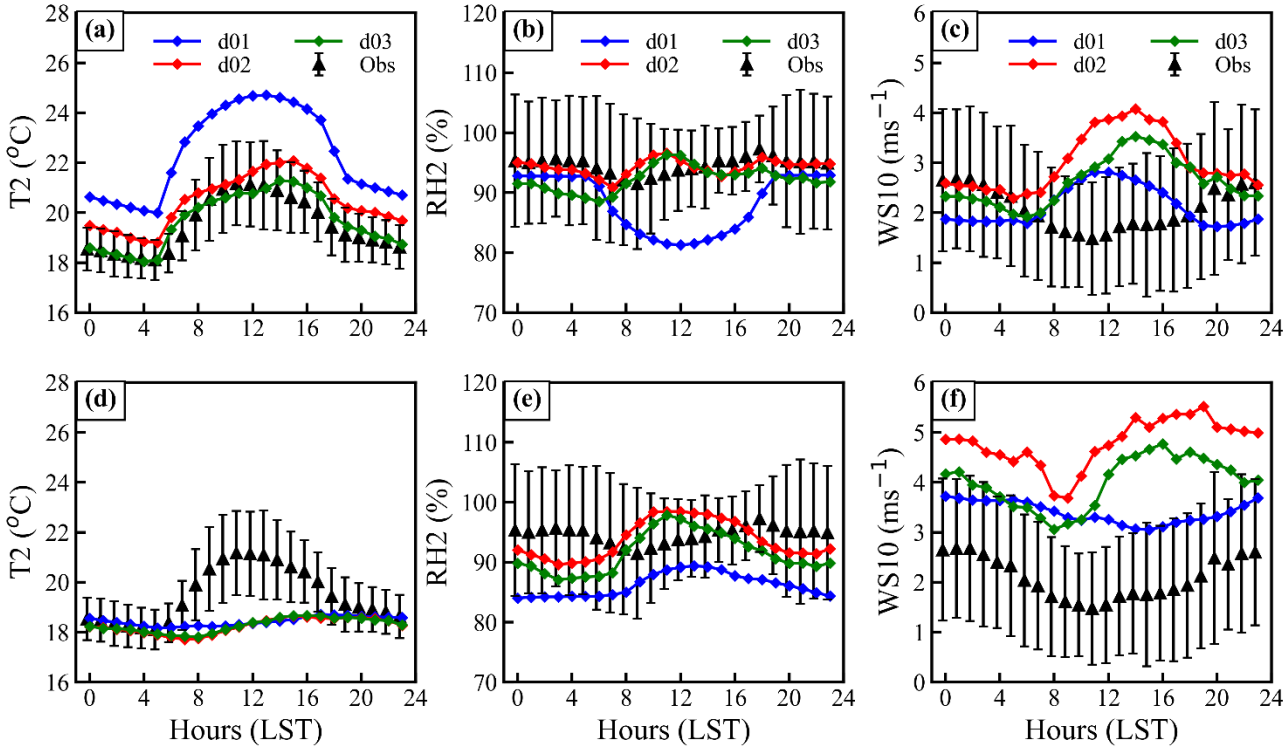

Figure 6: Mean diurnal variations of **(a)** 2m temperature: T2, **(b)** 2m relative humidity: RH2, and **(c)** 10m wind speed: WS10 from model simulations (d01, d02 and d03) and observations. Altitude adjusted variations are also shown (d–f).

Due to the complex terrains and the grid size of the model, the simulated altitude of the station could differ from the reality. In this study, the model underestimated station altitude by about 588m, 480m, and 270m in d01, d02, and d03 respectively. We performed an additional evaluation to explore how much improvement can be achieved by linearly interpolating the vertical profile of meteorological parameters to the actual altitude of the station (Figure d-f), as done in few previous studies (e.g. Mues et al., 2018). Analysis shows that correlations between model and observations do not show a clear improvement (e.g., T2: 0.35) by adjusting the altitude in model output except in case of WS10. Additionally, variability in temperature is not captured by the model over diurnal (Figure 6 a, d) as well as the day to day timescales i.e. r drops from 0.67 to 0.36 in d03 after the adjustment of altitude. As expected the altitude adjustment

385 does reduce bias in pressure. Nevertheless, reductions in mean biases are not achieved (Table S1), instead,
386 absolute values of biases show increase from 0.2 to 1.2, 2.4 to 3.1, 0.5 to 1.9, 0.7 to 1.6 in T2, RH2, WS10,
387 and Q2 in simulation d03. Besides thermal and mechanical interactions of the mountain surfaces with
388 atmosphere, local processes such as the evaporation, transpiration, etc. affect meteorological conditions in
389 the air just above the surface. A reduction in wind speed during the daytime is associated with the
390 competing effects of mountain-valley circulation due to the heating of the slopes versus synoptic-scale
391 flow (Solanki et al., 2019). To resolve such sub-grid scale processes, we emphasize that very high-
392 resolution simulations are needed, such as conducted here, to simulate in a satisfactory way the
393 meteorological variability. The analysis further highlights a need of accurate representation of the complex
394 topographical features rather than altitude adjusted estimations which lead to very limited improvements.
395 Here onwards we will discuss the evaluation without altitude adjustment until stated otherwise.

396 We evaluate the MB values in model simulations considering the benchmarks as suggested by Emery et
397 al. (2001). In the d03 simulation, MB values for both T2 (0.2^0C) and Q2 (-0.7) are found to be well within
398 the range of benchmark values: $\pm0.5^0$C for T2 and ±1.0 g kg^{-1} for Q2. It is important to note that biases in
399 T2 in the coarser simulations d01 (2.8^0C) and d02 (0.9^0C) are however higher as compared to the
400 benchmarks. MB values in T2 estimated here for the Himalaya are found to be slightly lower (+0.2) (-1.2
401 with altitude adjustment) than that over the Tibetan Plateau (-2 to -5) (Gao et al., 2015) and over
402 mountainous regions in the Europe (Zhang et al., 2013). Warmer bias in our case is due to underestimation
403 of Himalayan altitude, whereas, model overestimated terrain height over the Tibetan Plateau region giving
404 contrasting results. Further, the RMSE in wind speed here is lower (1.6–2.0 ms^{-1}) than that over
405 Kathmandu valley (2.2 ms^{-1}; Mues et al., 2018) and similar to benchmark (2.0 ms^{-1}). Mar et al. (2016) also
406 reported similar bias (2 ms^{-1}) in the 10m wind speed over Europe and average correlation of ~0.4–0.6 over
407 the Alps. As also seen here, simulating near surface diurnal winds remains challenging over complex
408 terrains, although the bias was reduced after including effects of the turbulent orographic form drag (Zhou
409 et al., 2017; 2019). Besides turbulent orographic form drag, it is suggested that wind speed is sensitive

towards boundary layer schemes (Yver et al., 2013; Zhou et al., 2019) and that more studies are needed to explore these aspects over the central Himalaya.

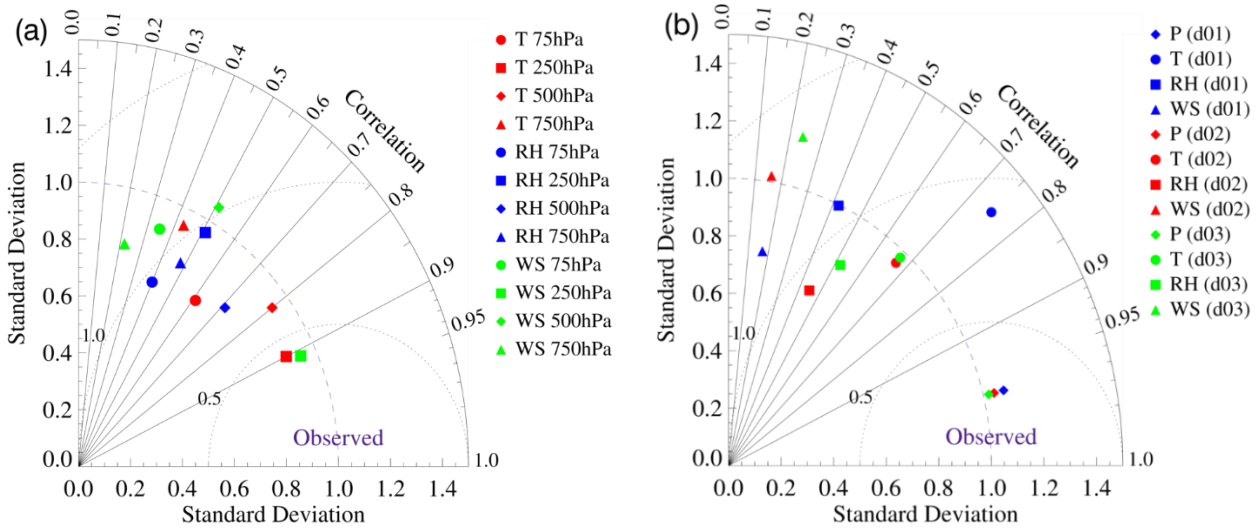

Figure 7: Taylor diagram with correlation coefficient, normalized standard deviation, and normalized root mean square difference (RMSD) error for (a) model performance at different pressure levels shown in Figure 3 for d01, and (b) the model simulated surface pressure, 2m temperature, RH and 10 m wind speed for different domains as shown in Figure 6a-c.

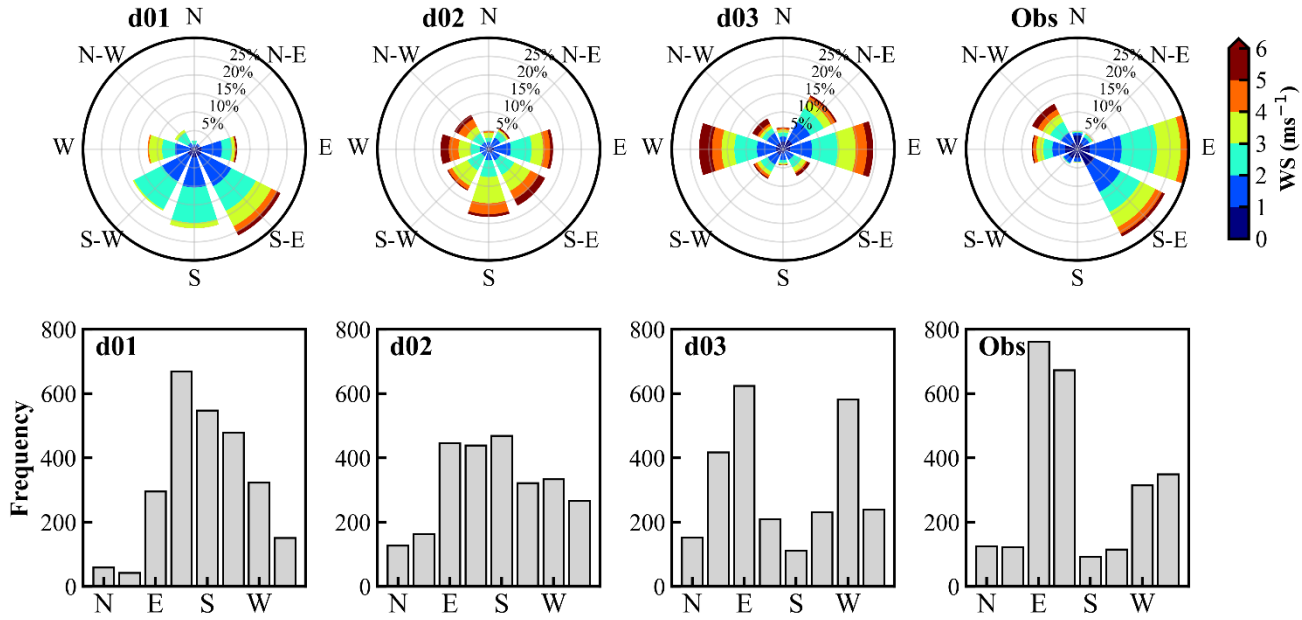

418

419

420 **Figure 8:** Comparison of the wind speed and direction as shown in form of wind rose (top panel), and
421 frequency distribution of wind direction (bottom row) from model simulations over the three domains
422 (d01, d02, d03) and observations (obs) during June-September 2011. Different colours and radius of wind
423 roses show the wind speed and frequency of counts respectively.

424

425 The wind direction is strongly influenced by the surrounding topography over the mountainous region and
426 the evaluation of the wind direction at horizontal resolution is shown Figure 8. The winds varying between
427 meteorological direction 337.5^0 to 22.5^0 are considered to be the Northerly and represented by N in the
428 frequency distribution and so on for other directions taking into account the clockwise meteorological
429 convention. The dominance of the wind flow over the observational site is easterly (30%) and south
430 easterly (26%) while 26% wind flows from the west and north-west. The frequency of southerly (539) and
431 south-westerly (SW, 481) are quite higher in d01 as compared to the observations (93 and 118
432 respectively), which decreases up to 109 and 232 in d03. Model is able to simulate the northerly and north-
433 easterly winds in d01 and d02, while, model simulates larger contribution of north easterly winds in d03

which is not present in the observations. The dominance of the summer monsoon seasonal easterly (30%) and south-easterly (27%) winds are clearly seen in the observation. The easterly component of the model simulated wind shows better agreement with observations on increasing the model resolution. Additionally, the model is able to simulate the westerly and north-westerly wind contribution in d02, whereas, the westerly component is over predicted by 10% in d03. The winds blowing from north, north-easterly, south and south-westerly are very weak (<2ms^{-1}) and are about ~15% of the total winds. Wind direction changed during transitions from high to low wind conditions during morning hours (7–10 h), and then low to high during evening (18–20 h). Overall, the simulated wind field in d03 are relatively in better agreement with observations than that of d01 and d02. This is further assessed in the section 3.5 using a finer resolution simulation through implementation of SRTM 3s terrain data.

3.4. Effect of feedback

In the preceding section, the results of the simulations carried out without any feedbacks (WRF-WF) from the finer resolution domain to its parent domain were presented. This WRF-WF experiment was conducted in such a way that it could explicitly account for the grid resolution effects on the model performance. The simulated meteorology with this model setup depicted different model performance in outermost coarse resolution domain d01 as compared to d02 and d03 (Figure 2 and 6). The model performance depends upon the boundary and initial conditions. Another model simulation is carried out in this section using the same configuration but with two-way interactive nesting and feedback (WRF-F) from daughter domain to its parent domain. The simulated meteorological parameters in higher nest are fed back to its parent domains and the boundary conditions replaced there. The model results over CH region in the regional scale simulation (d01) shows better agreement with the observations because of the feedback from high resolution nested simulation. The comparison of the simulated meteorological parameters (T2, RH2, and WS10) for outermost domain with the surface observations is presented in Figure 9 for both WRF-WF and WRF-F, and the effect of the feedback within outermost domain.

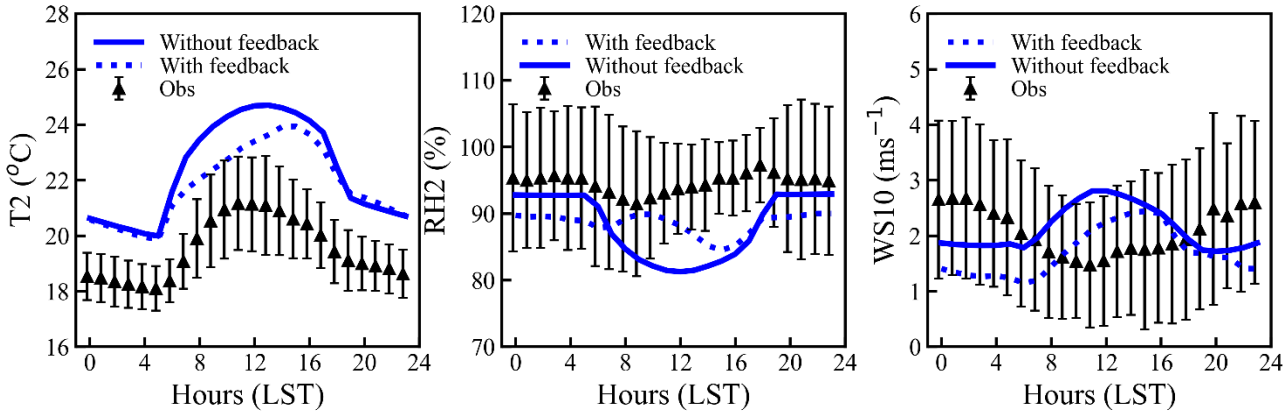

459 **Figure 9:** Diurnal variation of the T2, RH2, and WS10 from d01 without feedback (WRF-WF) and with
460 feedback (WRF-F) simulations.

461 The comparison of mean values (Table 2) shows a decrease in model bias for T2, RH2, and Q2 by 0.5 ^{0}C,
462 0.3%, and 0.2 gkg^{-1} respectively due to feedback from finer resolution simulations. Additionally,
463 correlations are found to be improved for RH2 and Q2 by 0.15 and 0.12 respectively due to feedback.
464 Nevertheless, smaller changes were seen in correlations for WS10 (by 0.05) and T2 (by -0.02) (Figure S2).
465 Variations in wind speed and direction shows an improvement in dominant flow direction e.g. easterly,
466 westerly and north-westerly (Figure S3). Effects of the feedback on surface pressure, T2, and RH2 at over
467 domain d01 is shown in Figure 10. Feedback effects is seen to be more pronounced over mountainous
468 region than over the plain region of IGP.

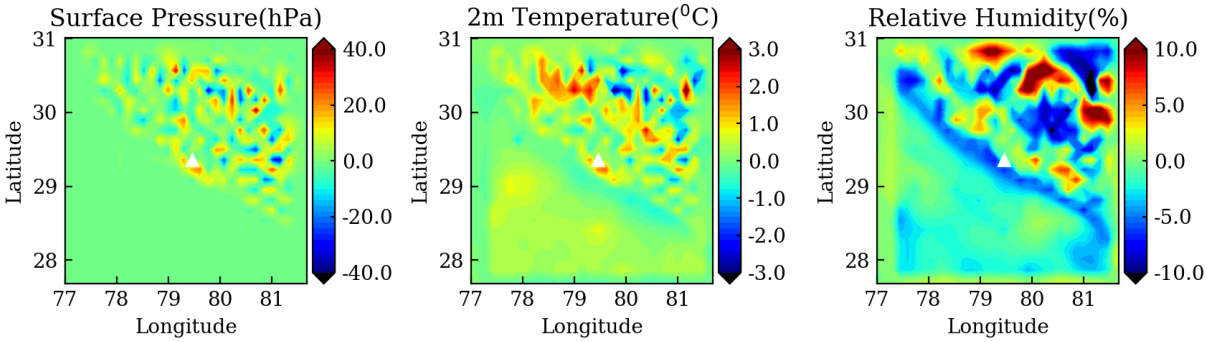

469

470 **Figure 10:** The effect of the two-way nesting on d01 is shown. The difference between the simulations
471 with feedback (WRF-F) and without feedback (WRF-WF) is shown for surface pressure, 2m temperature,
472 and 2m relative humidity.

Table 2: Comparison of the simulated meteorology for surface pressure (P), 2m Temperature (T2), 2m relative humidity (RH2), 10m wind speed (WS10) and 2m specific humidity (Q2) in two model simulations: WRF-WF and WRF-F at the observational site from outermost domain d01.

Parameters	Observed	WRF-WF	WRF-F
P (hPa)	801.4±2.4	869.6±2.6	858.9±2.5
T2 (^{0}C)	19.5±1.6	22.3±2.1	21.9±1.4
RH2 (%)	94.7±9.5	88.2±4.9	88.6±4.9
WS10 (ms^{-1})	2.1±1.4	2.1±1.1	1.7±1.3
Q2($g\ kg^{-1}$)	16.8±2.0	17.3±2.0	17.0±2.1

The feedback from the daughter domain to parent domain process mostly modifies the meteorology over the mountainous region within the domain. The effect of feedback is strikingly observed for the 2m temperature and the trend of diurnal variation of the relative humidity. The analyses of biases and correlations suggest an improvement in the model simulated pressure, temperature, and humidity through feedback from well resolved nests. This further underpins that better representations of Himalaya over local-scales can be adopted to simulate meteorology over regional-scale with lower biases over complex terrains in the domain. Nevertheless, further modelling studies alongside with more observations are needed to improve the model performance. We make further effort on the improvement of the wind speed and direction over the complex topography by implementing a high resolution (3s) topographical input in the model to evaluate further fine resolution features over Himalaya in the next section.

3.5. Inclusion of high resolution (3s) SRTM topography

Simulations described in previous sections were performed using the 30s (~1km) topographic data from the GMTED2010 (Danielson and Gesch, 2011). The resolution of this (30s or ~0.95km) is comparable to the highest resolution of the WRF simulation (d03). To evaluate influences of topographical features

over even finer scales on the wind flows over this highly complex terrain, topography input available at very high resolution (3s or ~90m) from the Shuttle Radar Topography Mission (SRTM3s) (Farr et al., 2007) has been implemented without altering the model configuration, except performing the simulation as d04 (~333m). Simulation with SRTM data at 1 km resolution did not differ significantly with the similar resolution simulation using GMTED2010 (GMTED hereinafter). For this experiment, model simulation is performed for 1 month only (September 2011). This simulation carried out without feedback and compared with the observation to check the effect of implementing high-resolution topography.

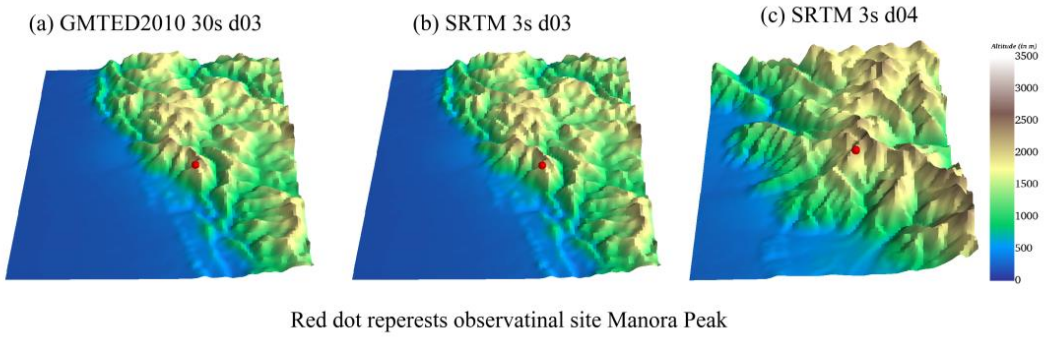

Figure 11: The topography from GMTED at 30s and SRTM at 3s in domain d03 and d04.

The differences of the topographic height between GMTED and SRTM3s as shown in Figure S4 shows that the differences are larger over the mountainous region which varies from -100 to +100m. The differences are lower in within d02 and d03 by changing input from GMTED to SRTM3s. The topography in the d04 get better resolved as depicted by sharp variations of mountain ridges and valleys using the SRTM3s as compared to the d03, as shown in the Figure 11, which could be smoothed out if the simulation was carried out with GMTED / or at 1 km with SRTM3s. The induced effects due the more resolved variability of topographic height in d04 can better simulate the local circulation of air mass. After including the SRTM3s topography, the MB and RMSE values for wind speed in d03 reduced slightly (~0.04 ms^{-1}). Additionally, wind directions also improved by ~1–2% for different directions after using the SRTM3s. Therefore, simulated 10 m wind direction in d04 is compared with the observations and d03 to investigate

the effect of including the SRTM3s topography. Surface pressure is seen to be simulated more realistically (809 hPa) and the dry bias in 2m relative humidity is improved by ~2%. Simulations of diurnal wind variations remain challenging (not shown here) even at finest resolutions considered here (d04) with updated topographic data (SRTM3s). The variations in winds are analysed by wind rose (Figure 12) and frequency distribution (Figure S5). A comparison is performed between d03 before and after using SRTM3s and the innermost nest d04 with SRTM3s. The fraction of north-easterly component in d04 with SRTM3s (5%) is found to be comparable to observation (6%), which was overestimated 19% (17%) in d03 with GMTED (SRTM3s). The southerly wind component consistently shows an agreement with the observations with increasing model resolution. The observation shows the prevalence of north-westerly (19%), easterly (24%), westerly (18%) and south-easterly (20%) winds and these are also seen to be dominant directions in the simulation d04, while occurrence of south-easterly winds is underestimated.

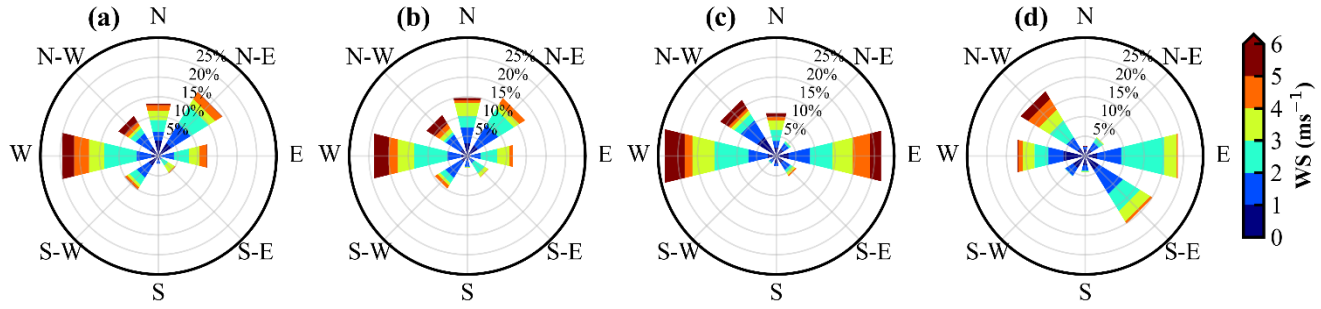

Figure 12: Wind roses (a) d03 using GMTED, (b-c) d03 and d04 using SRTM3s topography data, and (d) surface observation. The comparison of the wind speed and direction shown for the month September, 2011.

Simulation of the wind directions improved from d03 to d04 by using the SRTM3s topography being relatively in better agreement with observations, except certain wind directions such as south easterly. An improvement is noticed in simulated surface pressure, 2 m relative humidity and 10 m wind speed using the SRTM3s topography over the complex CH. The impact of the orographic variation with different resolution topographic data in RH (Figure S6) shows the differences are in range of -1 to 1% in d02 and -

3% to 3% in d03. Such variations are due to inclusion of the SRTM3s high resolution topographic data. Such multi-scale orographic variations are found to be key factors in meteorological simulation over complex terrains (e.g. Wang et al., 2020). The effects of the SRTM3s topographic static data is studied previously over other regions of the world (e. g. Teixeira et al., 2014; De Meij and Vinuesa, 2014). However, the daytime lower wind speed and the transition phases during morning and evening hours still remain a challenge even after using the high resolution (333m x 333m) nest. Such discrepancies between model and observations over the Himalayan region are suggested to be associated with still unresolved terrain features, besides the influences of input meteorological fields as well as the model physics on simulated atmospheric flows (e. g. Xue et al., 2014; Vincent et al., 2015).

4. Summary and Conclusions

In this study, the effects of spatial resolution on model simulated meteorology over the CH has been examined combining the WRF model with ground-based, balloon-borne observations during and intensive field campaign, and reanalysis datasets. Owing to the highly complex topography of the central Himalaya, model results show strong sensitivity towards the model resolution and adequate representation of terrain features. Model simulated meteorological profiles do not show much dependency on resolution except in the lower atmosphere, which is directly influenced by terrain induced effects and surface characteristics emphasizing the need also to evaluate various physics schemes over this region. The biases in 2 m temperature, relative humidity and pressure show a decrease on increasing the model resolution indicating a better resolved representation of topographical features. Diurnal variations in meteorological parameters also show better agreements on increasing the grid resolution. Although the surface pressure does not show a pronounced diurnal variation nevertheless the biases in simulated surface pressure reduce drastically over fine resolution simulations. Interpolation of coarser simulations (d01, d02) to the station altitude reduces the bias in surface pressure and temperature, but suppresses the diurnal variability. The results highlight the significance of accurately representing terrains at finer resolutions (d03). Model is

generally not able to reproduce the wind directions well, except some of the major components in all the simulations with varying resolutions. The directionality of the simulated winds show improvements over finer grid resolutions nevertheless reproducing the diurnal variability remains a challenge. Biases are stronger typically during daytime and also during transitions of low to high wind conditions and vice versa. This is attributed to the uncertainties in representing the interaction of slope winds with synoptic mean flow and local circulations, despite of an improved representation of terrain features. A sensitivity experiment with domain feedback turned ON shows that the feedback process can improve the representation of the CH in the simulation covering larger region of the northern Indian subcontinent. It is suggested that further improvements in the model performance are limited due to the lack of high-resolution topographical inputs biases through input meteorological fields, and model physics. Nevertheless, an implementation of a very high resolution (3s) topographical input using the SRTM data shows potential to reduce the biases related to topographical features to some extent.

Code and data availability

Observational data from the GVAX campaign is available freely (https://adc.arm.gov/discovery/#v/results/s/fsite::pgh.M). WRF is an open-source and publicly available model, which can be downloaded at http://www2.mmm.ucar.edu/wrf/users/download/get_source.html. . A zip file containing a) namelists for both pre-processor (WPS) as well as the WRF, b) 3 s resolution topography input prepared for the pre-processor, along with a README file describing details necessary to perform the simulations, has been archived at https://doi.org/10.5281/zenodo.3978569.

Author contributions

NS and AP designed and supervised the study. JS performed the simulations, assisted by NO and AS. JS, NO, AS analysed the model results and NVPKK, KR, SSG contributed to the interpretations. VRK

contributed significantly in conceiving and realizing the GVAX campaign. JS and NS wrote the first draft, and all the authors contributed to the manuscript.

Acknowledgement

This study has been supported by ABLN& C: NOBLE project under ISRO-GBP. We are thankful to Director ARIES, Nainital. We acknowledge NCAR for the WRF-ARW model, ECMWF for the ERA-Interim reanalysis data sets, ARM Climate Research Facility of U.S. Department of Energy (DOE) for availing the observations made during GVAX campaign. Computing resources from the Max Planck Computing and Data Facility (MPCDF) are acknowledged. N. Ojha acknowledges the computing resources - Vikram-100 HPC at Physical Research Laboratory (PRL), and valuable support from Duggirala Pallamraju and Anil Bhardwaj. Constructive comments and suggestions from the anonymous reviewers and the handling editor are gratefully acknowledged.

References

Bhutiyani, M.R., Kale, V.S. and Pawar, N.J.: Long-term trends in maximum, minimum and mean annual air temperatures across the Northwestern Himalaya during the twentieth century. Climatic Change, *85*, 59-177,https://doi.org/10.1007/s10584-006-9196-1.,2007.

Bonasoni, P., Cristofanelli, P., Marinoni, A., Vuillermoz, E. and Adhikary, B.: Atmospheric pollution in the Hindu Kush–Himalaya region: Evidence and implications for the regional climate. Mountain research and development, 32, 468-479, 2012.

Boyle, J. and Klein, S.A.: Impact of horizontal resolution on climate model forecasts of tropical precipitation and diabatic heating for the TWP-ICE period. Journal of Geophysical Research: Atmospheres, 115, https://doi.org/10.1029/2010JD014262, 2010.

Caya, D. and Laprise, R.: A semi-implicit semi-Lagrangian regional climate model: The Canadian RCM. Monthly Weather Review, 127, 341-362, https://doi.org/10.1175/1520-0493(1999)127<0341:ASISLR>2.0.CO;2, 1999.

607 Chen, F. and Dudhia, J.: Coupling an advanced land surface–hydrology model with the Penn State–NCAR
608 MM5 modeling system. Part I: Model implementation and sensitivity. Monthly Weather Review, 129,
609 569-585,https://doi.org/10.1175/1520-0493(2001)129<0569:CAALSH>2.0.CO;22001.

610 Cheng, W. Y. Y. and Steenburgh, W. J.: Evaluation of surface sensible weather forecasts by the WRF and the Eta
611 Models over the western United States, Weather Forecast., 20(5), 812–821, doi:10.1175/WAF885.1, 2005.

612 Chou, M.D. and Suarez, M.J.: An efficient thermal infrared radiation parameterization for use in general
613 circulation models, NASA Technical Memorandum No. 104606, Vol. 3, pp.85,1994.

614 Christensen, J.H., Christensen, O.B., Lopez, P., van Meijgaard, E. and Botzet, M.: The HIRHAM4
615 regional atmospheric climate model.DMI Scientific report, 4, p.51, 1996.

616 Danielson, J.J. and Gesch, D.B.: Global multi-resolution terrain elevation data 2010 (GMTED2010) (No.
617 2011-1073), US Geological Survey, 2011.

618 De Meij, A. and Vinuesa, J. F.: Impact of SRTM and Corine Land Cover data on meteorological
619 parameters using WRF, Atmos. Res., 143, 351–370, doi:10.1016/j.atmosres.2014.03.004, 2014.

620 Dee, D.P., Uppala, S.M., Simmons, A.J., Berrisford, P., Poli, P., Kobayashi, S., Andrae, U., Balmaseda,
621 M.A., Balsamo, G., Bauer, D.P. and Bechtold, P.: The ERA-Interim reanalysis: Configuration and
622 performance of the data assimilation system. Quarterly Journal of the royal meteorological society, 137,
623 pp.553-597, https://doi.org/10.1002/qj.828, 2011.

624 Deep, A., Pandey, C.P., Nandan, H. et al. Evaluation of ambient air quality in Dehradun city during 2011–
625 2014. J Earth Syst Sci 128, 96, doi:10.1007/s12040-019-1092-y, 2019.

626 Dimri, A.P., Chevuturi, A., Niyogi, D., Thayyen, R.J., Ray, K., Tripathi, S.N., Pandey, A.K. and Mohanty,
627 U.C.: Cloudbursts in Indian Himalayas: a review. Earth-science reviews, 168, pp.1-23,
628 https://doi.org/10.1016/j.earscirev.2017.03.006, 2017.

629 Ek, M.B., Mitchell, K.E., Lin, Y., Rogers, E., Grunmann, P., Koren, V., Gayno, G. and Tarpley, J.D.:
630 Implementation of Noah land surface model advances in the National Centers for Environmental
631 Prediction operational mesoscale Eta model. Journal of Geophysical Research: Atmospheres,
632 https://doi.org/10.1029/2002JD003296, 2003.

633 Emery, C., Tai, E., and Yarwood, G.: Enhanced meteorological modeling and performance evaluation for two Texas
634 ozone episodes, Tech. Rep. Prepared for The Texas Natural Resource Conservation Commission, ENVIRON
635 International Corporation, 2001.

636 Farr, T.G., Rosen, P.A., Caro, E., Crippen, R., Duren, R., Hensley, S., Kobrick, M., Paller, M., Rodriguez,
637 E., Roth, L. and Seal, D.: The shuttle radar topography mission, Reviews of geophysics, 45(2).
638 doi:10.1029/2005RG000183, 2007.

639 Foley, A.M.: Uncertainty in regional climate modelling: A review. Progress in Physical Geography, 34,
640 pp.647-670.https://doi.org/10.1177/0309133310375654, 2010.

641 Gao, Y., Xu, J. and Chen, D.: Evaluation of WRF mesoscale climate simulations over the Tibetan Plateau during
642 1979-2011, J. Clim., 28(7), 2823–2841, doi:10.1175/JCLI-D-14-00300.1, 2015.

643 Hanna, S. R. and Yang, R.: Evaluations of Mesoscale Models' Simulations of Near-Surface Winds, Temperature
644 Gradients, and Mixing Depths, J. Appl. Meteorol., 40(6), 1095–1104, doi:10.1175/1520-
645 0450(2001)040<1095:EOMMSO>2.0.CO;2, 2001.

646 Hart, K. A., Steenburgh, W. J. and Onton, D. J.: Model Forecast Improvements with Decreased Horizontal Grid
647 Spacing over Finescale Intermountain Orography during the 2002 Olympic Winter Games, Weather Forecast.,
648 20(4), 558–576, doi:10.1175/WAF865.1, 2005.

649 Hong, S.Y., Noh, Y. and Dudhia, J.: A new vertical diffusion package with an explicit treatment of
650 entrainment processes. Monthly weather review, 134, pp.2318-2341,
651 https://doi.org/10.1175/MWR3199.1, 2006.

652 Kain, J.S.: The Kain–Fritsch convective parameterization: an update. Journal of applied meteorology, 43,
653 pp.170-181, https://doi.org/10.1175/1520-0450(2004)043<0170:TKCPAU>2.0.CO;2 ,2004.

654 Kotamarthi, V.R.: Ganges Valley Aerosol Experiment (GVAX) Final Campaign Report. DOE/SC-ARM-
655 14-011, available at: https://www. arm. gov/publications/programdocs/doe-sc-arm-14-011. Pdf, 2013.

656 Kumar, R., Naja, M., Pfister, G.G., Barth, M.C. and Brasseur, G.P.: Simulations over South Asia using
657 the Weather Research and Forecasting model with Chemistry (WRF-Chem): set-up and meteorological
658 evaluation. Geoscientific Model Development, 5, p.321, https://doi.org/10.5194/gmd-5-321-2012, 2012.

659 Laprise, R. Regional climate modelling. Journal of Computational Physics, 227, pp.3641-3666.,
660 https://doi.org/10.1016/j.jcp.2006.10.024, 2008.

661 Lawrence, M.G. and Lelieveld, J.: Atmospheric pollutant outflow from southern Asia: a review.
662 Atmospheric Chemistry and Physics, 10, p.11017, https://doi.org/10.5194/acp-10-11017-2010, 2010.

663 Lee, T. J., Pielke, R. A., Kessler, R. C. and Weaver, J.: Influence of Cold Pools Downstream of Mountain Barriers
664 on Downslope Winds and Flushing, Mon. Weather Rev., 117(9), 2041–2058, doi:10.1175/1520-
665 0493(1989)117<2041:IOCPDO>2.0.CO;2, 1989.

Lelieveld, J., Bourtsoukidis, E., Brühl, C., Fischer, H., Fuchs, H., Harder, H., Hofzumahaus, A., Holland, F., Marno, D., Neumaier, M. and Pozzer, A.: The South Asian monsoon—pollution pump and purifier. Science, 361, pp.270-273, DOI:10.1126/science.aar2501, 2018.

Mar, K. A., Ojha, N., Pozzer, A. and Butler, T. M.: Ozone air quality simulations with WRF-Chem (v3.5.1) over Europe: Model evaluation and chemical mechanism comparison, Geosci. Model Dev., 9(10), 3699–3728, doi:10.5194/gmd-9-3699-2016, 2016.

Mass, C. F., Ovens, D., Westrick, K. and Colle, B. A.: DOES INCREASING HORIZONTAL RESOLUTION PRODUCE MORE SKILLFUL FORECASTS?: The Results of Two Years of Real-Time Numerical Weather Prediction over the Pacific Northwest, Bull. Am. Meteorol. Soc., 83(3), 407–430, doi:10.1175/1520-0477(2002)083<0407:DIHRPM>2.3.CO;2, 2002.

Meher, J.K., Das, L., Akhter, J., Benestad, R.E. and Mezghani, A.: 2017. Performance of CMIP3 and CMIP5 GCMs to simulate observed rainfall characteristics over the Western Himalayan region.Journal of Climate, 30, pp.7777-7799,*https://doi.org/10.1175/JCLI-D-16-0774.1*, 2017.

Mlawer, E.J., Taubman, S.J., Brown, P.D., Iacono, M.J. and Clough, S.A.: Radiative transfer for inhomogeneous atmospheres: RRTM, a validated correlated-k model for the longwave. Journal of Geophysical Research: Atmospheres, 102, pp.16663-16682. https://doi.org/10.1029/97JD00237, 1997.

Mues, A., Lauer, A., Lupascu, A., Rupakheti, M., Kuik, F. and Lawrence, M.G.: WRF and WRF-Chem v3. 5.1 simulations of meteorology and black carbon concentrations in the Kathmandu Valley. Geoscientific Model Development, 11, p.2067. https://doi.org/10.5194/gmd-11-2067-2018, 2018.

Naja, M., Bhardwaj, P., Singh, N., Kumar, P., Kumar, R., Ojha, N., Sagar, R., Satheesh, S. K., Krishna Moorthy, K., Kotamarthi, V. R., High-frequency vertical profiling of meteorological parameters using AMF1 facility during RAWEX–GVAX at ARIES, Nainital, Current Science, Vol. 111, No. 1, 132–140, 2016.

Nandargi, S. and Dhar, O.N.: Extreme rainstorm events over the northwest Himalayas during 1875–2010. Journal of Hydrometeorology, https://doi.org/10.1175/JHM-D-12-08.1 ,2012.

Ojha, N., Girach, I., Sharma, K., Nair, P., Singh, J., Sharma, N., Singh, N., Flemming, J., Inness, A. and Subrahmanyam, K.V.: Surface ozone in the Doon Valley of the Himalayan foothills during spring. Environ. Sci. Poll. Res., doi:10.1007/s11356-019-05085-2, 2019

Ojha, N., Naja, M., Singh, K.P., Sarangi, T., Kumar, R., Lal, S., Lawrence, M.G., Butler, T.M. and Chandola, H.C.: Variabilities in ozone at a semi-urban site in the Indo-Gangetic Plain region: Association

with the meteorology and regional processes. Journal of Geophysical Research: Atmospheres, https://doi.org/10.1029/2012JD017716, 2012.

Ojha, N., Pozzer, A., Rauthe-Schöch, A., Baker, A.K., Yoon, J., Brenninkmeijer, C.A. and Lelieveld, J.: Ozone and carbon monoxide over India during the summer monsoon: regional emissions and transport. Atmos. Chem. Phys, https://doi.org/10.5194/acp-16-3013-2016, 2016.

Pant, G.B., Pradeep Kumar, P., V. Revadekar, Jayashree, Singh, Narendra.: The Himalaya. https://doi.org/10.1007/978-3-319-61654-4, 2018.

Pant, P., Hegde, P., Dumka, U.C., Sagar, R., Satheesh, S.K., Moorthy, K.K., Saha, A. and Srivastava, M.K.: Aerosol characteristics at a high-altitude location in central Himalayas: Optical properties and radiative forcing. Journal of Geophysical Research: Atmospheres. https://doi.org/10.1029/2005JD006768, 2006.

Pervez, M.S. and Henebry, G.M.: Projections of the Ganges–Brahmaputra precipitation—Downscaled from GCM predictors. Journal of Hydrology, 517, pp.120-134.https://doi.org/10.1016/j.jhydrol.2014.05.016, 2014.

Rife, D. L. and Davis, C. A.: Verification of Temporal Variations in Mesoscale Numerical Wind Forecasts, Mon. Weather Rev., 133(11), 3368–3381, doi:10.1175/MWR3052.1, 2005.

Rupakheti, D., Adhikary, B., Praveen, P.S., Rupakheti, M., Kang, S., Mahata, K.S., Naja, M., Zhang, Q., Panday, A.K. and Lawrence, M.G., 2017.: Pre-monsoon air quality over Lumbini, a world heritage site along the Himalayan foothills. Atmos. Chem. Phys., 17, 11041-11063, https://doi.org/10.5194/acp-17-11041-2017, 2017.

Sarangi, T., Naja, M., Ojha, N., Kumar, R., Lal, S., Venkataramani, S., Kumar, A., Sagar, R. and Chandola, H.C.: First simultaneous measurements of ozone, CO, and NOy at a high-altitude regional representative site in the central Himalayas. Journal of Geophysical Research: Atmospheres, 119, pp.1592-1611. https://doi.org/10.1002/2013JD020631, 2014.

Sharma, A., Ojha, N., Pozzer, A., Mar, K. A., Beig, G., Lelieveld, J., and Gunthe, S. S.: WRF-Chem simulated surface ozone over south Asia during the pre-monsoon: effects of emission inventories and chemical mechanisms, Atmos. Chem. Phys., 17, 14393–14413, https://doi.org/10.5194/acp-17-14393-2017, 2017.

Sharma, S.S. and Ganju, A.: Complexities of avalanche forecasting in Western Himalaya—an overview. *Cold Regions Science and Technology*, *31*, pp.95-102.https://doi.org/10.1016/S0165-232X(99)00034-8, 2000.

Singh, N., Solanki, R., Ojha, N., Janssen, R.H., Pozzer, A. and Dhaka, S.K.: Boundary layer evolution over the central Himalayas from radio wind profiler and model simulations. Atmospheric Chemistry & Physics, https://doi.org/10.5194/acp-16-10559-2016, 2016.

Skamarock, W. C.,Klemp, J.B., Dudhia, J., Gill, D.O., Barker, D.M., Wang, W. and Powers, J.G.: A Description of the Advanced Research WRF Version 3. NCAR Technical Note NCAR/TN-475+STR, http://dx.doi.org/10.5065/D68S4MVH, 2008.

Solanki, R., Singh, N., Kumar, N.K., Rajeev, K. and Dhaka, S.K.: Time variability of surface-layer characteristics over a mountain ridge in the central Himalayas during the spring season. Boundary-layer meteorology, 158, pp.453-471, https://doi.org/10.1007/s10546-015-0098-5, 2016.

Solanki, R., Singh, N., Kiran Kumar, N. V. P., Rajeev, K., Imasu, R. and Dhaka, S. K.: Impact of Mountainous Topography on Surface-Layer Parameters During Weak Mean-Flow Conditions, Boundary-Layer Meteorol., 172(1), 133–148, doi:10.1007/s10546-019-00438-3, 2019.

Srivastava, A.K., Ram, K., Pant, P., Hegde, P. and Joshi, H.: Black carbon aerosols over Manora Peak in the Indian Himalayan foothills: implications for climate forcing. Environmental Research Letters, 7, p.014002, 2012.

Sun, X.B., Ren, G.Y., Shrestha, A.B., Ren, Y.Y., You, Q.L., Zhan, Y.J., Xu, Y. and Rajbhandari, R.: Changes in extreme temperature events over the Hindu Kush Himalaya during 1961–2015. Advances in Climate Change Research, https://doi.org/10.1016/j.accre.2017.07.001, 2017.

Taylor, K.E.: Summarizing multiple aspects of model performance in a single diagram. Journal of Geophysical Research: Atmospheres, 106, pp.7183-7192, https://doi.org/10.1029/2000JD900719, 2001.

Teixeira, J. C., Carvalho, A. C., Carvalho, M. J., Luna, T. and Rocha, A.: Sensitivity of the WRF model to the lower boundary in an extreme precipitation event-Madeira island case study, Nat. Hazards Earth Syst. Sci., 14(8), 2009–2025, doi:10.5194/nhess-14-2009-2014, 2014.

Tewari, M., Chen, F., Wang, W., Dudhia, J., LeMone, M.A., Mitchell, K., Ek, M., Gayno, G., Wegiel, J. and Cuenca, R.H.: Implementation and verification of the unified NOAH land surface model in the WRF model. In 20th conference on weather analysis and forecasting/16th conference on numerical weather prediction (Vol. 1115) , 2004,

754 Thompson, G., Rasmussen, R.M. and Manning, K.: Explicit forecasts of winter precipitation using an
755 improved bulk microphysics scheme. Part I: Description and sensitivity analysis. Monthly Weather
756 Review, 132(2), pp.519-542,https://doi.org/10.1175/1520-0493(2004)132<0519:EFOWPU>2.0.CO;2,
757 2004.

758 Tiwari, P.R., Kar, S.C., Mohanty, U.C., Dey, S., Sinha, P. and Shekhar, M.S.: Sensitivity of the Himalayan
759 orography representation in simulation of winter precipitation using Regional Climate Model (RegCM)
760 nested in a GCM. Climate Dynamics, 49(11-12), pp.4157-4170, https://doi.org/10.1007/s00382-017-
761 3567-3, 2017.

762 Tselioudis, G., Douvis, C. and Zerefos, C.: Does dynamical downscaling introduce novel information in
763 climate model simulations of precipitation change over a complex topography region? International
764 Journal of Climatology, 32, pp.1572-1578,https://doi.org/10.1002/joc.2360, 2012.

765 Vincent, C. L. and Hahmann, A. N.: The impact of grid and spectral nudging on the variance of the near-
766 surface wind speed, J. Appl. Meteorol. Climatol., 54(5), 1021–1038, doi:10.1175/JAMC-D-14-0047.1,
767 2015.

768 Wang, Y., Leung, L.R., McGREGOR, J.L., Lee, D.K., Wang, W.C., Ding, Y. and Kimura, F.: Regional
769 climate modeling: progress, challenges, and prospects. Journal of the Meteorological Society of Japan.
770 Ser. II, 82, pp.1599-1628,https://doi.org/10.2151/jmsj.82.1599, 2004.

771 Wang, Y., Yang, K., Zhou, X., Chen, D., Lu, H., Ouyang, L., Chen, Y., Lazhu and Wang, B.: Synergy of
772 orographic drag parameterization and high resolution greatly reduces biases of WRF-simulated precipitation in
773 central Himalaya, Clim. Dyn., 54(3), 1729–1740, doi:10.1007/s00382-019-05080-w, 2020.

774 Weisman, M.L., Skamarock, W.C. and Klemp, J.B.: The resolution dependence of explicitly modeled
775 convective systems. Monthly Weather Review, 125, pp.527-548, https://doi.org/10.1175/1520-
776 0493(1997)125<0527:TRDOEM>2.0.CO;2, 1997.

777 Wilby, R.L., Hay, L.E. and Leavesley, G.H.: A comparison of downscaled and raw GCM output:
778 implications for climate change scenarios in the San Juan River basin, Colorado. Journal of Hydrology,
779 225, pp.67-91, https://doi.org/10.1016/S0022-1694(99)00136-5, 1999.

780 Xue, Y., Janjic, Z., Dudhia, J., Vasic, R. and De Sales, F.: A review on regional dynamical downscaling
781 in intraseasonal to seasonal simulation/prediction and major factors that affect downscaling ability, Atmos.
782 Res., 147–148, 68–85, doi:10.1016/j.atmosres.2014.05.001, 2014.

Yver, C. E., Graven, H. D., Lucas, D. D., Cameron-Smith, P. J., Keeling, R. F. and Weiss, R. F.: Evaluating transport in the WRF model along the California coast, Atmos. Chem. Phys., 13(4), 1837–1852, doi:10.5194/acp-13-1837-2013, 2013.

Zadra, A., Caya, D., Côté, J.E.A.N., Dugas, B., Jones, C., Laprise, R., Winger, K. and Caron, L.P.: The next Canadian regional climate model. PhysCan, 64, pp.75-83, 2008.

Zhang, D. L. and Zheng, W. Z.: Diurnal cycles of surface winds and temperatures as simulated by five boundary layer parameterizations, J. Appl. Meteorol., 43(1), 157–169, doi:10.1175/1520-0450(2004)043<0157:DCOSWA>2.0.CO;2, 2004.

Zhang, Y., Sartelet, K., Wu, S. Y. and Seigneur, C.: Application of WRF/Chem-MADRID and WRF/Polyphemus in Europe - Part 1: Model description, evaluation of meteorological predictions, and aerosol-meteorology interactions, Atmos. Chem. Phys., 13(14), 6807–6843, doi:10.5194/acp-13-6807-2013, 2013.

Zhou, X., Beljaars, A., Wang, Y., Huang, B., Lin, C., Chen, Y. and Wu, H.: Evaluation of WRF Simulations With Different Selections of Subgrid Orographic Drag Over the Tibetan Plateau, J. Geophys. Res. Atmos., 122(18), 9759–9772, doi:10.1002/2017JD027212, 2017.

Zhou, X., Yang, K. and Wang, Y.: Implementation of a turbulent orographic form drag scheme in WRF and its application to the Tibetan Plateau, Clim. Dyn., 50(7–8), 2443–2455, doi:10.1007/s00382-017-3677-y, 2018.

Zhou, X., Yang, K., Beljaars, A., Li, H., Lin, C., Huang, B. and Wang, Y.: Dynamical impact of parameterized turbulent orographic form drag on the simulation of winter precipitation over the western Tibetan Plateau, Clim. Dyn., 53(1–2), 707–720, doi:10.1007/s00382-019-04628-0, 2019.